THE ASTROPHYSICAL JOURNAL, 409:697–704, 1993 June 1

OBSERVATIONS OF THE CRAB PULSAR AND NEBULA BY THE EGRET TELESCOPE ON THE *COMPTON GAMMA-RAY OBSERVATORY*

P. L. NOLAN,[1] Z. ARZOUMANIAN,[2] D. L. BERTSCH,[3] J. CHIANG,[1] C. E. FICHTEL,[3] J. M. FIERRO,[1]
R. C. HARTMAN,[3] S. D. HUNTER,[3] G. KANBACH,[4] D. A. KNIFFEN,[5] P. W. KWOK,[6] Y. C. LIN,[1]
J. R. MATTOX,[3,7] H. A. MAYER-HASSELWANDER,[4] P. F. MICHELSON,[1] C. VON MONTIGNY,[4]
H. I. NEL,[6,8] D. NICE,[2] K. PINKAU,[4] H. ROTHERMEL,[4] E. SCHNEID,[9] M. SOMMER,[4]
P. SREEKUMAR,[10] J. H. TAYLOR,[2] AND D. J. THOMPSON[3]
Received 1992 September 10; accepted 1992 December 7

ABSTRACT

The Crab pulsar and nebula were observed three times in 1991 April to June by the Energetic Gamma-Ray Experiment Telescope (EGRET) on the *Compton Gamma-Ray Observatory* (*CGRO*): April 23 to May 7, May 16 to 30, and June 8 to 15. The results of analysis of the gamma-ray emission in the energy range from 50 MeV to more than 10 GeV are reported. The observed gamma-ray light curve exhibits two peaks separated in phase by 0.40 ± 0.02, consistent with previous observations. The total pulsed emission from the Crab pulsar is found to be well represented by a power-law spectrum of the form

$$(4.11 \pm 0.16) \times 10^{-9}(E/274\ \mathrm{MeV})^{-2.15\pm0.04}\ \mathrm{photons\ cm^{-2}\ s^{-1}\ MeV^{-1}}\ ,$$

softer than the spectrum measured by *COS B* (Clear et al. 1987). The interpulse emission has a harder spectrum than either of the pulses. The evidence for pulsed emission above 5 GeV in the EGRET data is not conclusive. Unpulsed emission in the energy range 50 MeV to 5 GeV was detected, with an indication of a hardening of the unpulsed spectrum above about 1 GeV. There was a significant change in the light curve over the 2 months of these observations, although the shape of the spectrum remained constant.

Subject headings: gamma rays: observations — ISM: individual (Crab Nebula) — pulsars: individual (Crab Nebula)

1. INTRODUCTION

For many years it has been well established that the Crab pulsar and nebula are sources of both pulsed and unpulsed radiation from radio wavelengths to high-energy gamma rays. While the angular resolution of radio, optical, and X-ray telescopes is sufficient to separate the radiation from the pulsar and the nebula, the resolution of gamma-ray telescopes is insufficient for this purpose. X-ray emission from the pulsar is dominated by the DC nebular emission outside the "pulsed" portion of the light curve (Harden & Seward 1984). This suggests that the gamma-ray emission for the pulsar is also negligible in the off-pulse state, and we will proceed on that assumption. The Crab Nebula was among the first celestial sources of high-energy gamma rays to be identified (Kniffen et al. 1974; Lichti et al. 1980; Cawley et al. 1985). Recently, unpulsed emission from the Crab in the energy range 200–4000 GeV has been firmly established (Akerlof et al. 1989; Weekes et al. 1989; Vacanti et al. 1991). Pulsed gamma-ray emission from PSR 0531+21 in the energy range 1 to 1000 MeV has been previously established with balloon observations (Browning, Ramsden, & Wright 1971; Albats et al. 1972; Kinzer, Share, & Seeman 1973; McBreen et al. 1973; Parlier et al. 1973; Graser & Schönfelder 1982) and satellite observations with *SAS 2* (Thompson et al. 1977) and *COS B* (Bennett et al. 1977; Clear et al. 1987).

Models that have been proposed to explain the pulsed emission from the Crab pulsar generally fall into two categories. In the polar cap models (Daugherty & Harding 1982), an accelerator "gap" exists near each of the magnetic polar caps of the neutron star. Charged particles accelerated in this gap are injected into the strong magnetic field of the neutron star where an electron-positron pair cascade is initiated. Near the core of the emission cone, synchrotron radiation is dominant, while away from the core curvature radiation is believed to be dominant (Chiang & Romani 1992; Harding & Daugherty 1993).

In the outer magnetospheric gap models (Cheng, Ho, & Ruderman 1986a, b; Ho 1989) the accelerator gap forms further out in the magnetosphere and extends to near the light cylinder. Electrons and positrons are accelerated in these gaps and lose energy by curvature radiation. This curvature radiation interacts with lower energy (X-ray) photons to produce electron-positron pairs. Radiation above about 1 GeV is produced by inverse Compton scattering of the high energy pairs off the low-energy photons, and radiation below about 1 GeV is produced by synchrotron radiation of the lower energy electrons and positrons.

[1] Hansen Experimental Physics Laboratory, Stanford University, Stanford, CA 94305.
[2] Department of Physics, Princeton University, Princeton, NJ 08544.
[3] NASA/Goddard Space Flight Center, Code 662, Greenbelt, MD 20771.
[4] Max-Planck Institut fur Extraterrestrische Physik, 8046 Garching bei Munchen, Germany.
[5] Hampden-Sydney College, P.O. Box 862, Hampden-Sydney, VA 23943.
[6] NAS/NRC Postdoctoral Research Associate, NASA/GSFC, Code 662, Greenbelt, MD 20771.
[7] Compton Observatory Science Support Center, Computer Sciences Corporation, NASA/GSFC, Code 668.1, Greenbelt, MD 20771.
[8] On leave from Department of Physics, Potchefstroom University, Potchefstroom 2520, South Africa.
[9] Grumman Aerospace Corporation, Mail Stop A01-26, Bethpage, NY 11714.
[10] Universities Space Research Association, NASA/GSFC, Code 662, Greenbelt, MD 20771.

By contrast, the steady nebular emission mechanisms are believed to be better understood. Synchrotron radiation from very high-energy (VHE) electrons moving in a magnetic field accounts for the observed spectrum from IR to MeV energies (Kennel & Coroniti 1984) and inverse Compton scattering of IR to optical photons off the VHE electrons produces high-energy gamma rays up to the TeV energy range (Gould 1965; Rieke & Weekes 1969; De Jager & Harding 1992). Cheng et al. (1990) have proposed an alternative model in which VHE (> 100 GeV) gamma rays are produced by the decay of neutral pions that are produced by hadronic collisions. Most recently, Kwok, Cheng, & Lau (1991) have proposed another model in which most of the unpulsed gamma-ray emission is produced in a region just a few light cylinder radii beyond the pulsar and not in the extended nebula.

In this paper we report the results of a detailed analysis of observations of the Crab region made in 1991 by the EGRET telescope on the *Compton Gamma-Ray Observatory*. Because EGRET's effective area is about 20 times that of *COS B*, the EGRET observations allow a high-quality measurement of the emission from the pulsar and nebula in a relatively short exposure.

2. THE OBSERVATIONS

In the mode used for most of the EGRET observations the effective area of the telescope is about 1.0×10^3 cm^2 at 150 MeV and 1.5×10^3 cm^2 around 0.5–1 GeV for targets near the center of the field of view. The instrument has components typically used in high-energy gamma-ray telescopes; an anticoincidence system to discriminate against charged particle radiation, a multilevel thin-plate spark chamber system to convert gamma rays and determine the trajectories of the secondary electron-positron pair, a triggering telescope that detects the presence of the pair with the correct direction of motion, and an energy measuring calorimeter, which in the case of EGRET is a NaI(Tl) crystal. Descriptions of the instrument are given by Hughes et al. (1980) and Kanbach et al. (1988, 1989). Details of the instrument calibration, both before and after launch, are given by Thompson et al. (1993) and Nolan et al. (1992). The instrument is designed to be free of internal background and its calibration tests have verified that the internal background is at least an order of magnitude below the extragalactic diffuse gamma radiation.

For the observations reported here the *Compton Gamma-Ray Observatory* was in a nearly circular, approximately 450 km orbit with an inclination of 28°.5 and a period of ~93 minutes. Instrumental parameters for each of the observations are given in Table 1. Standard EGRET data processing (Bertsch et al. 1989; Thompson et al. 1993), including automatic computer processing as well as manual event reconstruction as needed, was performed to provide optimal estimates of the direction and energy of each photon. The EGRET exposure to the source as a function of time is not uniform because of occultations by the Earth, South Atlantic Anomaly passages, calibrations, and losses of data. The exposure shown in Table 1 is calculated from the known calibration of the telescope sensitivity as a function of operating mode and energy (Thompson et al. 1993) and the known times of occultations, etc. The April 23–May 7 exposure was composed of four short exposures (3–5 days) of the Galactic anticenter region; for this analysis we have combined these observations.

In this paper we will discuss only the results which can be obtained by studying photons with energy greater than 50 MeV. Although EGRET is sensitive down to about 30 MeV, the low-energy calibration is less certain. For spectral analysis we have used only Class A photon events (Thompson et al. 1993), the ones in which the spark chambers indicate that the secondary tracks are aiming toward the NaI calorimeter.

3. TEMPORAL ANALYSIS OF PSR 0531+21: GAMMA-RAY LIGHT CURVES

For each observation the arrival times of the detected gamma rays were transformed to Solar System Barycentric Time T with an accuracy of better than 0.1 ms, using the known radio position of the pulsar ($\alpha = 5^h34^m31^s.975$; $\delta = 22°0'52''.06$) corrected from epoch J2000 to the epoch of the EGRET observations. The phase ϕ of each gamma ray was determined from the pulsar rotational frequency f_0 and its first and second derivatives f_1, f_2 at epoch T_0 from

$$\phi = \phi_0 + \Delta T f_0 + \tfrac{1}{2}\Delta T^2 f_1 + \tfrac{1}{6}\Delta T^3 f_2 , \quad (1)$$

where $\Delta T = T - T_0$ and ϕ_0 is the phase offset; the phases are measured in fractions of a pulse period. The timing parameters were derived from contemporaneous, almost daily, 610 MHz radio observations of the pulsar using a 26 m antenna of the National Radio Astronomy Observatory at Green Bank, West Virginia. Table 2 lists the pulsar parameters used in the gamma-ray arrival time analysis. The parameter $\Delta T_\oplus$ is an equivalent pulse arrival time at the Earth's center of mass, expressed in milliseconds past 0^h UTC on the date specified for T_0, derived from radio observations corrected for interstellar dispersion. These values are based on a dispersion measure of 56.776 ± 0.005 cm^{-3} pc measured in 1992 May (Lundgren et al. 1992). The values of ϕ_0 are derived from the $\Delta T_\oplus$-values so that phase 0 corresponds to the peak of the dispersion-corrected radio pulse.

Gamma-ray light curves were created by phase binning gamma rays over a particular energy range that arrive from within an energy-dependent cone of half-angle θ_{max} about the pulsar's known position. The angle θ_{max}, determined from the energy-dependent instrumental point spread function, was

TABLE 1

EGRET OBSERVATION PARAMETERS FOR EACH OBSERVATION OF THE CRAB REGION

Observation Dates	Pointing Direction (α, δ)	Aspect Angle	Effective Area at 200 MeV (cm^2)	Exposure at 200 MeV (10^7 cm^2 s)
1991 Apr 23–May 7	86°.76, 22°.09	2°.9	1027	50.6
	89.80, 15.25	8.9		
	89.77, 15.24	8.9		
	83.52, 22.02	0.1		
1991 May 16–30	88.07, 17.14	6.4	894	41.0
1991 Jun 8–15	87.83, 12.47	10.3	751	16.7

TABLE 2

RADIO TIMING PARAMETERS USED IN THE GAMMA-RAY ARRIVAL TIME ANALYSIS OF PSR 0531+21

Observation Period	Epoch T_0 JD-2,400,000.5	$\Delta T_\oplus$ (ms)	f_0 (s^{-1})	f_1 (10^{-10} s^{-2})	f_2 (10^{-20} s^{-3})
1991 Apr 23–May 7	48367	10.0	29.9493820573442	−3.77660	0.745
1991 May 16–30	48367	10.0	29.9493820573442	−3.77660	0.745
1991 Jun 8–15	48449	24.2	29.9467067038240	−3.77575	1.06

chosen so that 67% of the photons originating from the source are within the acceptance cone. The angle θ_{max} is well approximated by

$$\theta_{max} = 5.^{\circ}85 \times (E/100\ \mathrm{MeV})^{-0.534}\ .$$

This is similar to the procedure used to optimize the signal-to-noise in the *COS B* analysis of the Crab and other pulsars (Clear et al. 1987; Buccheri et al. 1983). Figure 1 shows the resultant phase histograms for each of the EGRET observations for photons with $E > 100$ MeV. Figure 2 shows phase histograms, summed over all of the EGRET observations of the Crab region, for several different energy intervals. By cross-correlation and by fitting model functions, we find that the phase separation of the two peaks is 0.40 ± 0.02, consistent with that observed by *COS B* (Wills et al. 1982; Clear et al. 1987). The first peak occurs at the same phase in all energy bands; the phase difference between the 50–200 MeV and 200–1000 MeV peaks is less than 150 μs (2 σ), consistent with the measurement errors.

There is more detail visible, particularly in Figure 1*d*, than there was in the *COS B* light curve. For this reason we have chosen to divide the on-pulse portion of the light curve into five sections, indicated by the vertical dashed lines in Figure 1

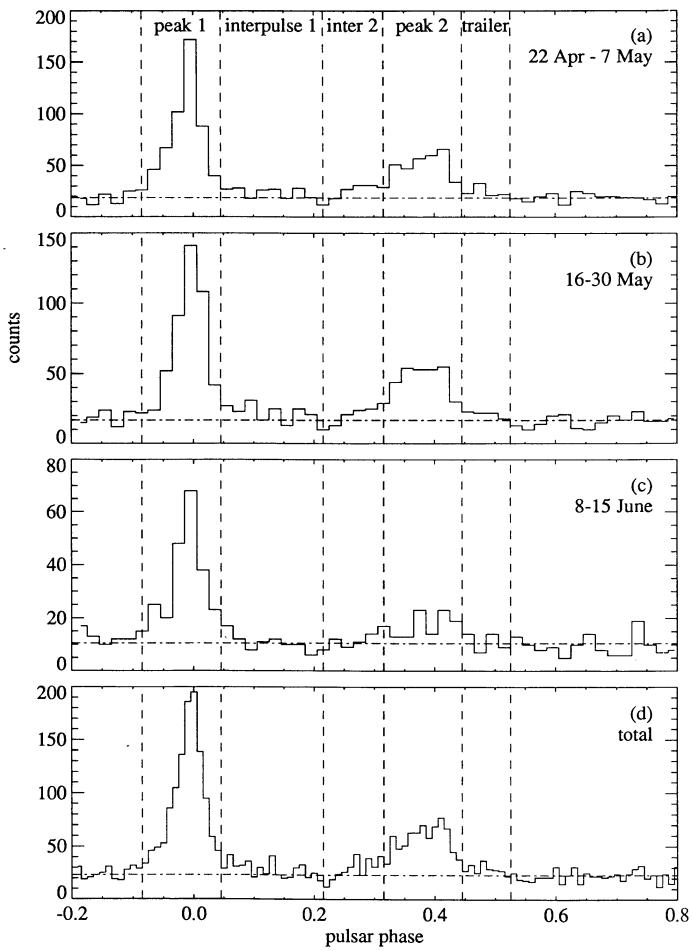

FIG. 1.—(*a–c*) Gamma-ray phase histograms of photons with $E > 100$ MeV for each of the EGRET observations of the Crab region. Phase 0 is defined by the timing solution derived from the radio observations. The vertical dashed lines indicate phase boundaries used in the spectral analysis. The horizontal dashed lines show the average number of counts in the off-pulse portion of the light curve. There are 50 phase bins. (*d*) A similar histogram for all three observations combined, with 100 phase bins.

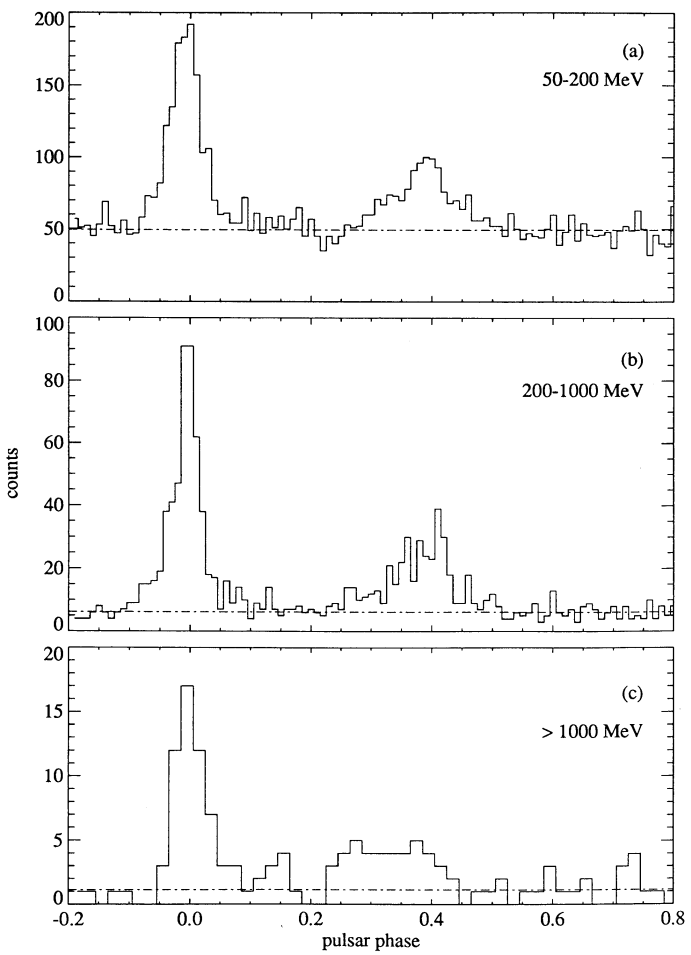

FIG. 2.—Gamma-ray phase histograms, summed over all of the EGRET observations of the Crab in 1991 April–June, for three different energy intervals. There are 100 phase bins in (*a*) and (*b*), and 50 in (*c*).

TABLE 3

DEFINITION OF PHASE INTERVALS FOR THE CRAB PULSAR

Region	Phase Interval
First pulse	0.915–0.045
Interpulse 1	0.045–0.215
Interpulse 2	0.215–0.315
Second pulse	0.315–0.445
Trailer	0.445–0.525
Total pulse	0.915–0.525
Off-pulse	0.525–0.915

and the values in Table 3. There is a direct analogy between these phase boundaries and those used by Grenier, Hermsen, & Clear (1988) in studying the Vela pulsar. The statistical significance of the interpulse 1, interpulse 2, and trailer emission above background is at least 3 σ in the light curve of the combined observations. In the first and second observations considered separately, these three features all have at least 2 σ significance. In the third observation neither the trailer nor the interpulse regions are detectable. However, due to the shorter exposure in the third observation, the 2 σ upper limits are consistent with the detections in the first two observations. The second peak is much broader than it appears to be in the *COS B* data, probably because of the better signal-to-noise ratio in EGRET. The "interpulse 2" and "trailer" portions of the light curve could be treated as part of the second peak, whose total width would be 0.31 in phase, but, as will be shown below, there is considerable variation in the spectrum within that interval. The "peak 2" in the EGRET light curve is what ratio astronomers usually call the "interpulse," while the "interpulse" is the radio astronomers' "bridge."

It is apparent from Figure 1 that the strength of the second peak decreased with respect to the first between the first two observations and the third. This may be related to the variation observed by *COS B* over a period of years (Wills et al. 1982; Özel & Mayer-Hasselwander 1984; Clear et al. 1987). For photons with energy greater than 50 MeV, the ratio of the background-subtracted counts in the two peaks (P_2/P_1) is 0.45 ± 0.05, 0.52 ± 0.06, and 0.29 ± 0.08 for the three observations. These numbers cannot be compared directly with the *COS B* ratios since the boundaries of the phase bins are slightly different. When we use the same bin boundaries as *COS B*, the ratios are 0.39 ± 0.04, 0.38 ± 0.04, and 0.20 ± 0.06. In either case the evidence for variation is strong. Kanbach (1990) fitted a sinusoidal function with a period of 14 years to the *COS B* and *SAS 2* values of this ratio. He speculated that the variation might be due to nutation of the neutron star. When we add the EGRET data points to the earlier data, the variation is approximately consistent with a sinusoid with a period of 13.5 ± 0.7 years, as shown in Figure 3. Clearly it will require several years of further observation to decide if this variation is truly periodic. The sharp decrease in P_2/P_1 in less than a month has not been seen before.

We performed statistical tests to see if the light curves for the first two observations were truly identical. Both a Kolmogorov-Smirnov test and a χ^2 test, based on a normalized difference between the two phase histograms, suggested by Buccheri (1992), yield the same results: There is no indication of a difference between the first two observations ($\chi^2 = 40.0$ for 48 degrees of freedom). On the other hand, the difference between the second and third observations is marked ($\chi^2 = 88.0$; probability $= 3.8 \times 10^{-4}$).

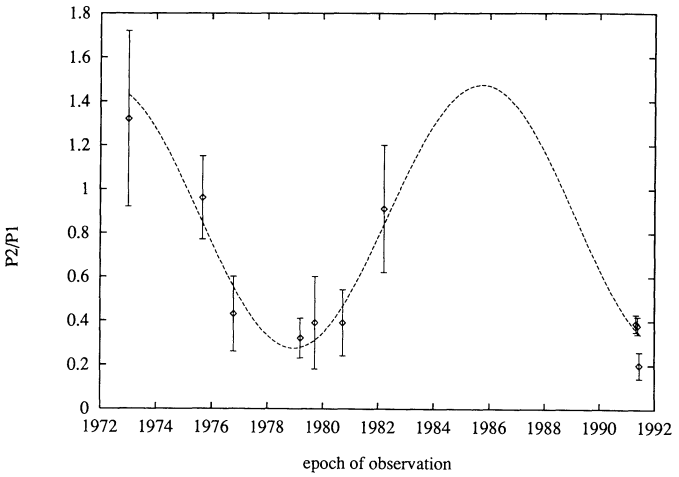

FIG. 3.—Variation in the ratio of the two peaks in the Crab light curve for $E > 50$ MeV. The 1991 data points are from this paper. The 1973 data point was measured by *SAS 2* (Kanbach 1990). The other data points were measured by *COS B* (Clear et al. 1987). The dashed curve is a sinusoidal function with a period of 13.5 yr.

4. THE SPECTRUM OF THE PULSED EMISSION FROM PSR 0531+21

The background corrected differential photon spectrum for the pulsed phase interval (0.915 to 0.525) was determined as follows. First the data set was divided into nine observed energy intervals. For each energy interval, the quantity n_j, the estimated number of counts from the pulsed source in each observed energy interval, was computed, where

$$n_j = n_p - n_{up}\Delta\phi_p/\Delta\phi_{up} ,$$

n_{up} is the number of counts observed in the unpulsed phase interval, $\Delta\phi_p/\Delta\phi_{up}$ is the ratio of the pulsed phase interval to the unpulsed interval, and n_p is the number of counts observed in the pulsed phase interval. The number of counts, either pulsed or unpulsed, was determined by the number of counts observed within an energy dependent acceptance cone centered on the known position of the source. The true pulsed energy spectrum $I_p(E)$ differs from the observed n_j because of several factors. EGRET's detection efficiency is not uniform over the observed energy range, and the energy resolution is fairly broad and varies with energy and angle of incidence. Also the acceptance cone is energy-dependent and represents a compromise between including as many source counts and excluding as many background counts as possible.

The general approach here is to fit a specified model (either a power law or a broken power law) to the data rather than attempt a deconvolution. We begin with a source model $I(E, \lambda)$, where λ represents a set of free parameters. For a single power-law model, λ represents two parameters: a spectral index and a normalization. For a broken power-law model, λ represents four parameters: two spectral indices, a break energy, and a normalization. Using the EGRET instrumental response functions (Thompson et al. 1993), we calculate model source counts $m_j(\lambda)$ for each of the nine observed energy intervals. The

parameters of the model are adjusted to minimize the function

$$\chi^2 = \sum_j (1/w_j)[n_j - m_j(\lambda)]^2 ,$$

where w_j is the estimated variance of the jth energy band. Initially w_j is set equal to $n_j + n_{up}(\Delta\phi_p/\Delta\phi_{up})^2$. After the minimum is found, the w_j are replaced by $m_j + n_{up}(\Delta\phi_p/\Delta\phi_{up})^2$ and χ^2 is minimized again. The process is repeated until it converges. Based on an analysis of data taken in flight, the effective area for the 50–70 MeV band has been decreased from the value found by calibration, and the statistical weight of that band has been decreased.

Figure 4*a* shows the derived pulsed spectrum for the summation of all of the EGRET observations of the Crab in 1991. The data are well represented, between 50 MeV and 10 GeV, by a single power-law spectrum of

$$dN/dE = (4.11 \pm 0.16) \times 10^{-9}(E/274\ \text{MeV})^{-2.15\pm0.04} \times \text{photons cm}^{-2}\ \text{s}^{-1}\ \text{MeV}^{-1} . \quad (2)$$

The energy scale factor, 274 MeV, in equation (2), is chosen so that the statistical errors in the power-law index and the overall normalization are uncorrelated. This flux is the instantaneous flux averaged over the "pulsed" phase interval. The pulsed flux averaged over the whole period is 0.61 of this value. The average spectrum observed by *COS B* (Clear et al. 1987) had a spectral index of 2.00 ± 0.10. The difference is only marginally significant.

The combined EGRET observations provide a sufficient number of photons that analysis of the spectrum in each of the five pulsed emission regions defined in Table 3 is possible. The results are shown in Figure 4*b*–4*f*. Table 4 lists the spectral indices and integrated flux values, for $E > 50$ MeV, for the different phase regions of pulsed emission. The "interpulse" and "trailer" emission was too weak to allow good spectrum fits in the individual observations, but fits can be obtained when the three observations are summed. The two peaks, however, can be studied in the individual observations. There is no significant variation in the spectral index of the two peaks from one observation to another, although the flux varies. There is, however, a significant variation in the spectral index from one part of the pulse to another. In particular, the interpulse emission is harder than that of either of the pulses and the trailer is softer. The structure of this variation is similar to that observed in the Vela pulsar (Grenier et al. 1988; Kanbach et al. 1993b).

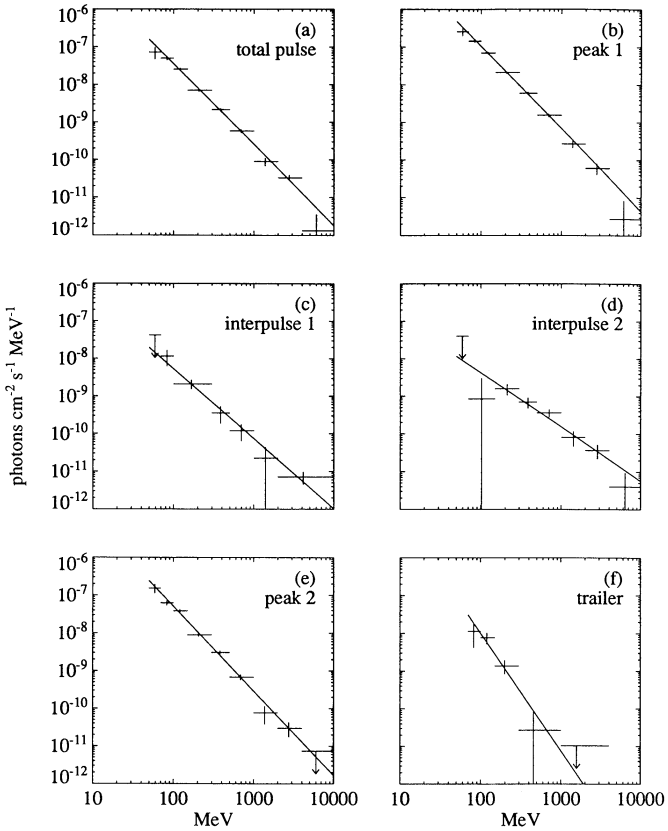

FIG. 4.—Differential photon spectrum of the combined observations of PSR 0531+21 from (*a*) the total pulse, (*b*) the first pulse, (*c*) interpulse 1, (*d*) interpulse 2, (*e*) the second pulse, and (*f*) the trailer. The various regions are defined by the phase boundaries in Table 3. Table 4 gives the derived spectral parameters. The background and unpulsed emission have been subtracted by the method described in the text. The error bars are statistical. The upper limits are 2 σ.

The pulsation is undetectable at very high energy. Above 200 GeV strong upper limits have been established for pulsed

TABLE 4

PULSED GAMMA RAY FLUXES AND SPECTRAL INDICES WITH STATISTICAL UNCERTAINTIES DURING EACH EGRET OBSERVATION OF THE CRAB REGION DURING 1991

Observation Period	Apr 23–May 7	May 16–30	June 8–15	Sum
A. Instantaneous Pulsed Flux (10^{-6} photons cm^{-2} s^{-1}, $E > 100$ MeV)				
First pulse	9.9 ± 0.5	7.8 ± 0.4	8.7 ± 0.7	8.8 ± 0.3
Interpulse 1	...	...	...	0.6 ± 0.1
Interpulse 2	...	...	...	1.0 ± 0.2
Second pulse	4.8 ± 0.4	4.1 ± 0.3	2.5 ± 0.4	4.1 ± 0.2
Trailer	...	...	...	0.5 ± 0.1
Total pulsed flux	3.7 ± 0.2	2.9 ± 0.2	2.4 ± 0.3	3.1 ± 0.1
B. Spectral Index				
First pulse	2.15 ± 0.06	2.24 ± 0.07	2.21 ± 0.10	2.19 ± 0.04
Interpulse 1	...	...	...	1.87 ± 0.17
Interpulse 2	...	...	...	1.43 ± 0.13
Second pulse	2.24 ± 0.09	2.22 ± 0.09	2.40 ± 0.21	2.25 ± 0.06
Trailer	...	...	...	3.12 ± 0.52
Total pulsed flux	2.10 ± 0.07	2.21 ± 0.07	2.15 ± 0.13	2.15 ± 0.04

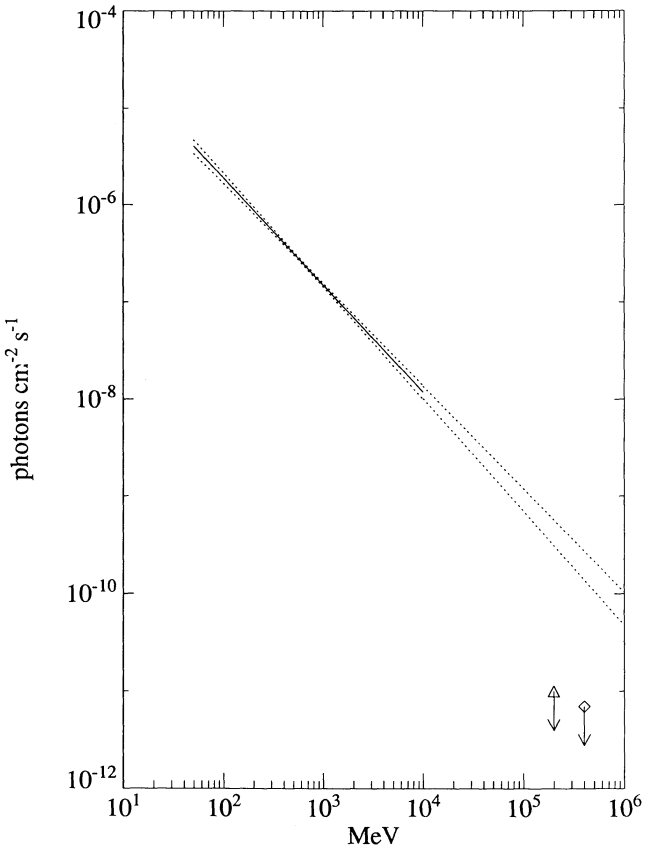

FIG. 5.—Integral photon spectrum of the pulsed component of PSR 0531+21. The solid line is the integral of the best-fit EGRET spectrum (averaged), and the dotted lines represent $\pm 1\ \sigma$ statistical uncertainties. The symbols are 99% significance upper limits (*diamond*, Vacanti et al. 1991; *triangle*, Akerlof et al. 1989).

emission (Vacanti et al. 1991, and references therein). In Figure 5 some of these limits are compared with the extrapolation of our pulsed spectrum from Figure 4*a*. The extrapolation exceeds the upper limits by a factor of at least 15. It is possible that the break in the pulsed spectrum may occur in the EGRET energy band, but the evidence is not definite. In the combined observations there were 12 photons with energy greater than 5 GeV whose apparent directions were consistent with the Crab's position. Of these eight had phases within the "total pulsed" interval and the other four were in the "off-pulse" interval. The last data point in Figure 4*a* is based on the 10 photons which fall in the 4–10 GeV band (seven pulsed, three off-pulse). The derived net pulsed flux is consistent with zero, but it is also consistent with the best-fit power law. This model predicts 8.6 pulsed counts, while we detect 2.3 ± 3.8.

There is no comprehensive model which explains all the features of the pulsed radiation from the Crab pulsar. Both the polar cap (Harding & Daugherty 1993) and the outer gap (Ho 1992) models predict a fall-off at energies above a few GeV, consistent with the EGRET observations. Both models indicate that the spectrum in the EGRET energy range should show some curvature rather than fitting a straight power law. The EGRET statistics do not allow us to distinguish these models from each other. Unexplained features include the 0.4 phase separation of the two peaks and the time variability of the P_2/P_1 ratio. Proposed models must also deal with the variation of the spectrum with phase, the simultaneity of the pulses across the electromagnetic spectrum, and the difference in shape of the two pulses.

5. UNPULSED GAMMA-RAY EMISSION FROM THE CRAB REGION

Following the convention used by Clear et al. (1987), we use the phase interval 0.525–0.915 (defined as off-pulse in Table 3) to represent the unpulsed emission from the Crab pulsar and nebula. Since the flux in each phase interval depicted in Figure 1 includes contributions from the diffuse gas emission as well as from the pulsar and the nebula, the determination of the background contribution due to the unpulsed flux must proceed differently than for the purely pulsed component. First, the number of source counts in each energy interval was determined by a maximum likelihood analysis which includes a point source at the Crab's location, a model of the diffuse background, and the presence of the other known nearby point sources in the field, Geminga (Bertsch et al. 1992) and PKS 0528+134 (Hunter et al. 1993). Data were excluded during the time of the June 11 solar flare (Kanbach et al. 1993a). Then a spectral model was fitted to the estimated unpulsed source counts by the procedure described above.

The model of the diffuse gamma-ray background was based on the interaction of cosmic rays with interstellar gas and the interstellar radiation field. The primary gamma ray production processes are nucleon-nucleon interaction, electron bremsstrahlung, and inverse Compton scattering. The expected diffuse gamma-ray emission is calculated from a detailed knowledge of the interstellar gas together with a model of the cosmic-ray density distribution (Kniffen & Fichtel 1981; Fichtel & Kniffen 1984; Bertsch et al. 1993). The cosmic-ray density is assumed to be almost proportional to the local gas density because of the confinement of cosmic rays by interaction with interstellar magnetic fields embedded in the interstellar gas.

Given the diffuse background model, the source strength for the Crab emission was determined by simultaneously optimizing the likelihood probability function with the normalization of the background model and the source strengths of the three point sources as free parameters (Mattox et al. 1993b).

For this gas model of the diffuse background, the differential photon spectrum for the unpulsed phase interval is shown in Figure 6. The best-fit single power law has the form

$$dN/dE = (9.1 \pm 0.8) \times 10^{-9}(E/118\ \mathrm{MeV})^{-2.93 \pm 0.15} \times \mathrm{photon\ cm^{-2}\ s^{-1}\ MeV^{-1}}. \quad (3)$$

The integral unpulsed flux implied by this spectrum is $(7.7 \pm 0.8) \times 10^{-7}$ photons cm^{-2} s^{-1} for $E > 100$ MeV. Above 1 GeV the observed data points in Figure 6 appear to be well above the fitted model. However, the statistical significance of this excess is only 2.4 σ, so it must be regarded as an indication, rather than a positive detection. Changing the model spectrum to a broken power law produced a better fit, but not conclusively. (χ^2 decreased from 15.12 with 6 degrees of freedom to 9.70 with 4 degrees of freedom.) To check for sensitivity to possible errors in the background model, we repeated this analysis with a uniform ("flat") background model and the estimated spectral parameters changed by less than 1 σ.

As already noted, the angular resolution of gamma-ray telescopes such as EGRET is not sufficient to separate the nebular

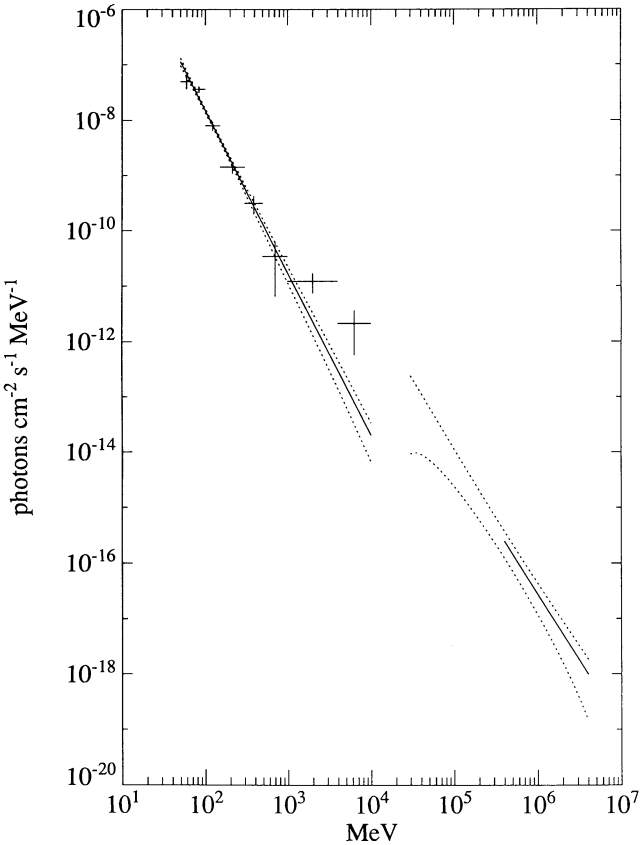

FIG. 6.—Differential spectrum of the unpulsed emission. The EGRET spectrum (data points) comes from the off-pulse interval defined in Table 3. The solid line from 50 MeV to 10 GeV is the best-fit single power-law model. The dotted lines surrounding it are $\pm 1\ \sigma$ statistical uncertainties. The solid line from 4×10^5 to 4×10^6 MeV is from Vacanti et al. (1991). The dotted lines surrounding it are based on $\pm 1\ \sigma$ statistical uncertainties and 50% systematic uncertainty in the normalization.

emission from the pulsar emission based on position. It is usually assumed that the steady emission in the off-pulse phase interval is due to the nebula (see however, Kwok et al. 1991). The unpulsed nebular emission from radio to gamma-ray energies is believed to be due to relativistic protons or electrons injected into the nebula from the pulsar. Pinkau (1970) proposed that protons interacting with the interstellar medium could be the source of the gamma rays.

The unpulsed component in the 1 to 20 MeV range (Graser & Schonfelder 1982; McConnell et al. 1993) matches well with the synchrotron spectrum extended to these energies. The measured polarization of the radio and optical emission supports the sychrotron interpretation. Above 30 MeV, *SAS 2* reported detection of an unpulsed component (Thompson et al. 1977). In the *COS B* data, Clear et al. (1987) found that about 53% of the emission in the 50 to 500 MeV band is unpulsed with a spectral index of 2.7 ± 0.3, and they also reported an upper limit for the flux in the 500 MeV to 3 GeV band. Recently Mattox, De Jager, & Harding (1993a) reanalyzed the *COS B* observations to investigate the possibility that the unpulsed emission is variable. They found no evidence of variability. Our spectrum in the 50–500 MeV range is consistent with the Clear et al. (1987) observation, while our marginal detection for $E > 500$ MeV is below their upper limit.

Gould (1965) suggested that inverse Compton scattering of the synchrotron radiation by the relativistic electrons should produce TeV gamma rays. The Whipple Observatory group (Weekes et al. 1989; Vacanti et al. 1991) have reported significant detection of a strong unpulsed component from the Crab Nebula in the energy range 400 GeV to 4 TeV with a spectral index of 2.4 ± 0.3. This spectrum is shown in Figure 6. Recently, De Jager & Harding (1992) have reexamined the synchrotron-self Compton model and calculated the high-energy gamma-ray spectrum expected. For a realistic magnetic field distribution model they find a TeV flux and spectral index consistent with the Whipple observations. Their results also indicate that the unpulsed flux in the 50–500 MeV range reported by Clear et al. (1987) cannot be accounted for by inverse Compton scattering. They interpret this emission as an extension of the synchrotron spectrum at lower energies and, assuming the same nebular magnetic field distribution used to compute the inverse Compton spectrum, find that the electron spectrum must extend up to at least 10^{16} eV to produce this radiation. Since this electron energy is very near the maximum available from the full vacuum potential across the pulsar polar cap and is at the maximum theoretical limits of acceleration at the pulsar wind shock, De Jager & Harding (1992) suggest that the upper end of the *COS B* unpulsed flux must be near the upper end of the synchrotron spectrum. They predict a hardening of the spectrum above about 1 GeV as the inverse Compton component becomes more important. The possible hardening of the unpulsed emission in the energy range 500 MeV to 5 GeV (Fig. 6) is consistent with this prediction. With more observations it should be possible to measure the spectrum in this transitional energy band and thus help to determine some properties of the nebula, such as the magnetic field distribution and the maximum particle energy.

6. SUMMARY AND CONCLUSIONS

The observations of the Galactic anticenter region by EGRET in 1991 have allowed a detailed analysis of the Crab spectrum in several phase intervals. The total exposure on the Crab region obtained with EGRET for the three observations reported here is already more than the exposure obtained by *COS B* during 6.7 years of operation. This has provided important new information about the emission of high-energy gamma-rays from the Crab region. In particular,

1. The pulsed spectrum is similar in all observations. The light curve shows variation on a scale of a month, with the second peak about 50% weaker in the June observation.

2. The new level of detail visible in the average light curve for the summed observations shows that it contains features similar to the Vela Pulsar light curve: two different interpulse regions with hard spectra, and a soft trailer after the second pulse.

3. The EGRET observations have confirmed the power-law nature of the pulsed emission spectrum measured by *COS B*. The EGRET spectrum for the pulsed phase interval, after subtraction of the DC component, is well-represented by a power law with spectral index 2.15 ± 0.04 throughout the range 50 MeV to 5 GeV. The spectrum is slightly softer than the spectral index of 2.00 ± 0.10 reported by *COS B*. The analysis indicates that the evidence for pulsed emission above 4 GeV is inconclusive. There must be a break in the pulsed spectrum somewhere above GeV to agree with upper limits above 200 GeV.

4. The unpulsed emission has also been found to be consis-

tent with a power law with spectral index 2.93 ± 0.15 over the energy range from 50 MeV to 1 GeV with some indication of hardening of the spectrum above 1 GeV. The apparent hardening is consistent with synchrotron-self Compton models, and it matches well with an extrapolation of the spectrum measured at TeV energies.

Occasional observations of the Crab region with the EGRET instrument will continue for the next several years. These observations will add to an already valuable Crab gamma-ray data base.

The authors are grateful for the many contributions to the EGRET project made prior to their deaths by E. Barrie Hughes and Robert Hofstadter. We also thank R. Buccheri for his χ^2 test. The EGRET team gratefully acknowledges support from the following: Bundesministerium fur Forschung und Technologie grant 50 QV 9065 (M. P. E.); NASA grant NAG5-1742 (H. S. C.), NASA grant NAG5-1605 (S. U.); and NASA contract NAS5-31210 (G. A. C.). The NRAO is operated by Associated Universities, Incorporated, under a cooperative agreement with the National Science Foundation.

REFERENCES

Akerlof, C., DiMarco, J., Levy, H., Meyer, D., Radusewicz, P., Tschirhart, R., Yama, Z., & MacCallum, C. 1989, in Proc. Gamma-Ray Observatory Science Workshop, ed. W. N. Johnson (Greenbelt, MD: NASA), 4-49
Albats, P., Frye, G. M., Zych, A. D., Mace, O. B., Hopper, V. D., & Thomas, J. A. 1972, Nature, 240, 221
Bertsch, D. L., et al. 1989, in Proc. Gamma-Ray Observatory Science Workshop, ed. W. N. Johnson (Greenbelt, MD: NASA), 2-52
———. 1992, Nature, 357, 306
Bertsch, D. L., Dame, T. M., Fichtel, C. E., Hunter, S. D., Sreekumar, P., Stacey, J. G., & Thaddeus, P. 1993, in preparation
Bennett, K., et al. 1977, A&A, 61, 279
Browning, R., Ramsden, D., & Wright, P. J. 1971, Nature Phys. Sci., 232, 99
Buccheri, R. 1992, private communication
Buccheri, R., et al. 1983, A&A, 128, 245
Cawley, M. F., et al. 1985, Proc. 19th Internat. Cosmic-Ray Conf. (La Jolla), 1, 131
Cheng, K. S., Cheung, T., Lau, M. M., Yu, K. N., & Kwok, P. W. 1990, J. Phys. G, 16, 1115
Cheng, K. S., Ho, C., & Ruderman, M. 1986a, ApJ, 300, 500
———. 1986b, ApJ, 300, 522
Chiang, J., & Romani, R. W. 1992, in Compton Observatory Science Workshop, ed. C. R. Schrader, N. Gehrels, & B. Dennis (NASA Conf. Pub. 3137), 237
Clear, J., Bennett, K., Buccheri, R., Grenier, I. A., Hermsen, W., Mayer-Hasselwander, H. A., & Sacco, B. 1987, A&A, 174, 85
Daugherty, J. K., & Harding, A. K. 1982, ApJ, 252, 337
De Jager, O. C., & Harding, A. K. 1992, ApJ, 396, 615
Fichtel, C. E., & Kniffen, D. A. 1984, A&A, 134, 13
Gould, R. J. 1965, Phys. Rev. Lett., 15, 577
Graser, U., & Schönfelder, V. 1982, ApJ, 263, 677
Grenier, I. A., Hermsen, W., & Clear, J. 1988, A&A, 204, 117
Harding, A. K., & Daugherty, J. K. 1992, in Proc. Los Alamos Workshop on Physics of Isolated Pulsars, ed. K. Van Riper, R. I. Epstein, & C. Ho (Cambridge: Cambridge Univ. Press), in press
Harnden, F. R., & Seward, F. D. 1984, ApJ, 283, 279
Ho, C. 1989, ApJ, 342, 396
Hughes, E. B., et al. 1980, IEEE Trans. Nucl. Sci., NS-27, 364
Hunter, S. D., et al. 1993, ApJ, in press
Kanbach, G. 1990, in The EGRET Science Symposium, ed. C. Fichtel et al. (NASA Conf. Pub. 3071), 101
Kanbach, G., et al. 1988, Space Sci. Rev., 49, 69
———. 1989, in Proc. Gamma-Ray Observatory Science Workshop, ed. W. N. Johnson (Greenbelt, MD: NASA), 2-1
———. 1993a, A&AS, in press
———. 1993b, in preparation
Kennel, C. F., & Coroniti, F. V. 1984, ApJ, 283, 710
Kinzer, D. A., Share, G. H., & Seeman, N. 1973, ApJ, 180, 547
Kniffen, D. A., Hartman, R. C., Thompson, D. J., Bignami, G. F., Fichtel, C. E., Tümer, T., & Ögelman, H. 1974, Nature, 251, 397
Kniffen, D. A., & Fichtel, C. E. 1981, ApJ, 250, 389
Kwok, P. W., Cheng, K. S., & Lau, M. M. 1991, ApJ, 379, 653
Lichti, G. G., et al. 1980, Non-Solar Gamma Rays, Advances in Space Exploration, ed. R. Cowsik & R. D. Wills (Oxford: Pergamon), 7, 49
Lundgren, S. C., Cordes, J. M., Foster, R., Hankins, T., Ulmer, M., & Garasi, C. 1992, in Proc. Compton Observatory Science Workshop, ed. C. R. Schrader, N. Gehrels, & B. Dennis (NASA Conf. Pub. 3137), 260
Mattox, J., De Jager, O. C., & Harding, A. K. 1993a, in Proc. Los Alamos Workshop on Physics of Isolated Pulsars, ed. K. Van Riper, R. I. Epstein, & C. Ho (Cambridge Univ. Press), in press
Mattox, J. R., et al. 1993b, in preparation
McBreen, B., Ball, S. E., Campbell, M., Greisen, K., & Koch, D. 1973, ApJ, 184, 571
McConnell, M., et al. 1993, in Proc. Los Alamos Workshop on Physics of Isolated Pulsars, ed. K. Van Riper, R. I. Epstein, & C. Ho (Cambridge: Cambridge Univ. Press), in press
Özel, M. E., & Mayer-Hasselwander, H. A. 1984, in Data Analysis in Astronomy, ed. V. Di Gesù et al. (NY: Plenum), 81
Nolan, P. L., et al. 1992, IEEE Trans. Nucl. Sci., NS-39, 993
Parlier, B., et al. 1973, Nature Phys. Sci., 242, 117
Pinkau, K. 1970, Phys. Rev. Lett., 25, 603
Rieke, G. H., & Weekes, T. C. 1969, ApJ, 15, 577
Thompson, D. J., Fichtel, C. E., Hartman, R. C., Kniffen, D. A., & Lamb, R. C. 1977, ApJ, 213, 252
Thompson, D. J., et al. 1993, ApJS, in press
Vacanti, G., et al. 1991, ApJ, 377, 467
Weekes, T. C., et al. 1989, ApJ, 342, 379
Wills, R. D., et al. 1982, Nature, 296, 723